Geochemical Perspectives Letters

Contribution of the nuclear field shift to kinetic uranium isotope fractionation

A.R. Brown[1], Y. Roebbert[2], A. Sato[3], M. Hada[3], M. Abe[3,4], S. Weyer[2], R. Bernier-Latmani[1]*

https://doi.org/10.7185/geochemlet.2333

Abstract

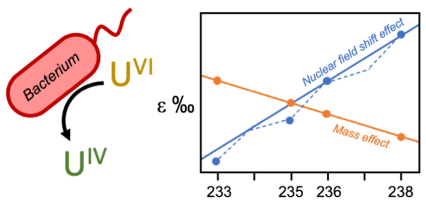

Isotopic fractionation of heavy elements (*e.g.*, >100 amu) often invokes the nuclear field shift effect, which is due to the impact of the elements' large nuclei on electron density. In particular, it has been explicitly described for uranium (U) at equilibrium and during kinetic isotope fractionation in abiotic mercury reactions. By following the fractionation of ^{233}U, ^{235}U, ^{236}U and ^{238}U during the enzymatic reduction of hexavalent U to tetravalent U by the bacterium *Shewanella oneidensis*, we provide the first direct evidence of the nuclear field shift effect during biologically controlled kinetic isotope fractionation. Here, we observed the odd-even staggering trend between fractionation factors of each isotope and their nuclear masses, and show that fractionation factors are correlated better with the nuclear volume than the mass. Additionally, by computing the relative contributions of the conventional mass-dependent effect (vibrational energy) and the mass-independent effect (nuclear field shift), we demonstrate that the experimental nuclear field shift effect is smaller than the calculated equilibrium value and that this discrepancy is responsible for the kinetic fractionation factor being lower than that predicted at equilibrium.

Received 17 March 2023 | Accepted 8 September 2023 | Published 9 October 2023

Introduction

Redox transformations of uranium (U) lead to measurable fractionation of U isotopes. These fractionations typically result in the enrichment of the heavy isotope (^{238}U) in the reduced state, the opposite direction of the mass-dependent fractionation observed for light elements (Andersen *et al.*, 2017). Further, isotope exchange reactions have revealed anomalous fractionations of the odd-mass isotopes, *i.e.* ^{233}U and ^{235}U, which deviate from the linear relationship between mass and fractionation magnitude observed for the even-mass isotopes (Fujii *et al.*, 1989a, 1989b; Nomura *et al.*, 1996). This odd-even staggering was observed to correlate with the isotope shifts in the atomic spectra of the isotopes, and specifically with the nuclear field shift, whereby distortions in the sizes and shapes of nuclei (the nuclear volume) between isotopes impact the electron densities surrounding the nucleus, which in turn impact ground state electronic energies. This led to the inclusion of a nuclear field shift (NFS) term in the theoretical calculation of isotopic enrichment factors for heavy elements (Bigeleisen, 1996).

These isotope exchange reactions have been assumed to be equilibrium processes (Fujii *et al.*, 2009), and the nuclear field shift effect (NFSE) itself has thus far been calculated only for equilibrium exchange reactions (Bigeleisen, 1996; Moynier *et al.*, 2013). Furthermore, given that hexavalent U (U^{VI}) reduction in the laboratory and nature display the same direction of fractionation as predicted for equilibrium (Bigeleisen, 1996; Schauble, 2007; Stirling *et al.*, 2015), the nuclear field shift was also implicated for kinetically controlled reactions (Bopp *et al.*, 2010; Basu *et al.*, 2014, 2020; Stirling *et al.*, 2015). However, no direct evidence for the NFSE during kinetic U reduction has been provided to date; *i.e.* the odd-even staggering in the fractionation of isotopes has not yet been observed.

Whilst the NFSE has been observed during abiotic and kinetic fractionations of Hg isotopes (Zheng and Hintelmann, 2010), to our knowledge, there is no evidence of the NFSE during the biotic fractionation of any element. Indeed, mass-independent isotope fractionation of Hg has been observed in biological systems (*e.g.*, in fish) but this has been attributed to the nuclear spin effects or photochemical reactions, rather than to the NFSE (Kritee *et al.*, 2009; Epov *et al.*, 2011).

Results

Here, we provide direct evidence of the NFSE during kinetic isotope fractionation *via* the enzymatic reduction of U^{VI} by the bacterium, *Shewanella oneidensis* strain MR-1. To achieve this result, we measured the simultaneous fractionation of ^{233}U, ^{235}U, ^{236}U and ^{238}U throughout this reaction and report the odd-even staggering trend only previously seen during abiotic chemical exchange reactions.

1. École Polytechnique Fédérale de Lausanne (EPFL), Environmental Microbiology Laboratory, CH-1015 Lausanne, Switzerland
2. Institute of Mineralogy, Leibniz University Hannover, D-30167 Hannover, Germany
3. Department of Chemistry, Tokyo Metropolitan University, Tokyo, Japan
4. Department of Chemistry, Hiroshima University, Hiroshima, Japan
* Corresponding author (email: rizlan.bernier-latmani@epfl.ch)

First, we prepared an isotope mix of the IRMM-184 natural U standard and the IRMM-3636 ^{233}U and ^{236}U "double spike", typically used to correct for instrumental mass bias during MC-ICP-MS (multi-collector inductively coupled plasma mass spectrometry) analyses of the $^{238}U/^{235}U$ ratio. The isotope mix was supplied to anoxic reactors containing *S. oneidensis* MR-1 in the presence of lactate, which serves as the electron donor for U^{VI} reduction, and 30 mM sodium bicarbonate, which complexes the U^{VI} to give aqueous tri- and dicarbonate species (Fig. S-1). This well documented reaction leads to the reductive precipitation of solid phase U^{IV} through the extracellular transfer of electrons *via* enzymes on the bacterial surface (Wall and Krumholz, 2006).

Here, we show that for duplicate systems, aqueous U concentrations decreased over several days, indicative of the precipitation of U^{IV} (Fig. 1a). This reaction was accompanied by the fractionation of ^{238}U and ^{235}U, such that the light ^{235}U was enriched in the residual unreacted aqueous U^{VI}, as evidenced by the progressively negative $\delta^{238}U$ values (Fig. 1b). This fractionation is well described by Rayleigh distillation models, from which the derived fractionation factors (ε) are ~1 ‰. These values are very typical for these biologically mediated reactions and demonstrate the sequestration of the isotopically heavy U^{IV} product from the reactants, as shown previously for U isotope fractionation (Basu *et al.*, 2014; Stirling *et al.*, 2015; Stylo *et al.*, 2015).

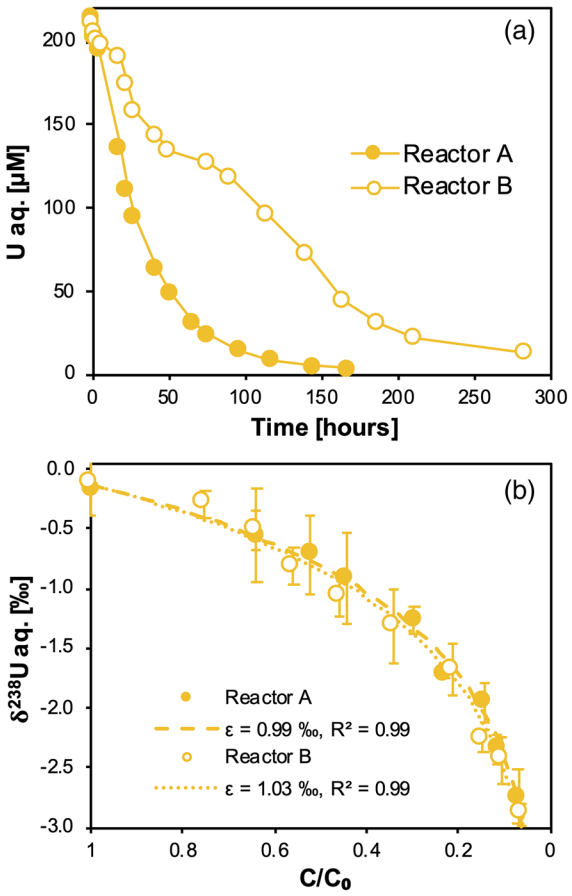

Figure 1 **(a)** Concentration of aqueous U (representing U^{VI}), as a function of time, in reactors containing 200 µM U^{VI} and 30 mM sodium bicarbonate incubated with *S. oneidensis*. Filled and open symbols depict duplicate reactors. **(b)** $\delta^{238}U$ values for aqueous U reported as a function of the remaining aqueous U fraction. Filled and open symbols depict duplicate reactors and error bars show 2 standard deviations of the mean of triplicate measurements. Rayleigh model curves for each duplicate reactor are shown in dashed lines, along with their corresponding isotope enrichment factors (ε). See Supplementary Information for definition of $\delta^{238}U$.

The inclusion of ^{233}U and ^{236}U in the isotope mix allowed the fractionation of these additional odd- and even-mass isotopes to be monitored (Fig. S-2), in order to reveal the presence of the odd-even staggering that would implicate the role of the NFSE in the fractionation of U isotopes. Here, three-isotope plots revealed that the fractionation behaviour did not conform to the theoretical relationship for mass-dependent isotope fractionation (Figs. 2, S-3). Total fractionation between ^{236}U and ^{235}U was larger than expected for a mass difference of 1 amu, compared to the fractionation of ^{238}U and ^{235}U ($\Delta m = 3$ amu). Additionally, the fractionation between the two odd-isotopes, ^{233}U and ^{235}U ($\Delta m = 2$ amu) was less than expected compared to the fractionation of ^{238}U and ^{235}U. These anomalous fractionations are consistent with those observed previously for U isotopes in chemical exchange reactions, in which fractionation factors for each isotope scale better with the mean square nuclear charge radii rather than the isotope mass (Fig. S-4), indicating that the nuclear volume dominates the fractionation (Fujii *et al.*, 2009; Moynier *et al.*, 2013). Here, we also observe odd-even isotope staggering in the relationship between isotopic mass and fractionation factors and demonstrate this same trend between ε and the mean square nuclear charge radii (Fig. 3) (Angeli and Marinova, 2013). Thus, in addition to the direction of U isotope fractionation, these data offer strong evidence that the NFSE is also responsible for the mass-independent nature of isotope fractionation observed for this kinetic reaction.

To probe whether the observed mass-independent fractionation arose from ongoing abiotic equilibrium isotope exchange between reactant U^{VI} and the solid U^{IV} product, or from the kinetically controlled enzymatic reduction, we performed isotope exchange experiments between isotopically heavy aqueous U^{VI} carbonate (initial $\delta^{238}U = \sim 5$ ‰) and the U^{IV} products of the bioreduction experiment (initial $\delta^{238}U = 0$ ‰). Here, we controlled the U speciation to be the same as during bioreduction using the same solution composition and ensured no further biologically mediated redox change by inactivating bacterial cells *via* sonication. Over several months, we observed the progressive depletion of the heavy ^{238}U from aqueous U^{VI} (Fig. S-5) as it

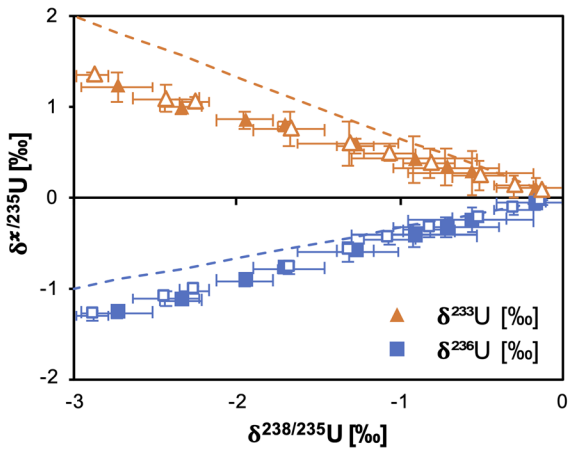

Figure 2 Three-isotope plots for delta values of all samples. Filled and open symbols depict duplicate reactors and error bars show two standard deviations of the mean of triplicate measurements. Dashed lines represent theoretical relationships for mass-dependent fractionation.

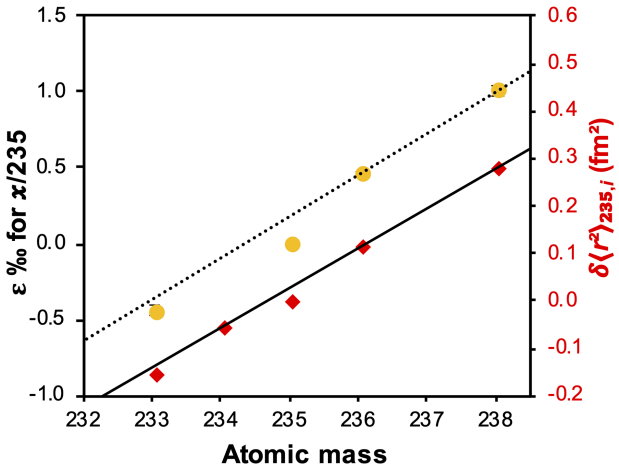

Figure 3 Fractionation factors (ε) for each atomic mass. Symbols and error bars depict the mean and standard deviation of duplicate reactors. Where not visible, the error is within the size of the symbol. Mean square nuclear charge radii ($\delta\langle r^2\rangle_{235,i} = \delta\langle r^2\rangle_i - \delta\langle r^2\rangle_{235}$) for each atomic mass were taken from Angeli and Marinova (2013). The lines represent linear regressions of ε and $\delta\langle r^2\rangle_{235,i}$ for even-mass numbers only.

became enriched in the U^{IV} species, as expected. However, this process was minor and theoretical equilibrium was not achieved (*e.g.*, $\varepsilon^{eq} = 1.1$ to 2.7 ‰ from *ab initio* calculation; Table S-1). That is to say, the aqueous U^{VI} remained isotopically heavier than the U^{IV} solid phase after several months, compared with the few days required to generate isotopically heavy U^{IV} during bioreduction. Additionally, the slight increase in aqueous U suggests that at least part of the decrease in $\delta^{238}U_{aq}$ may have actually been due to release of light U from the solid, rather than isotope exchange between dissolved and solid phases. These observations suggest that, whilst ongoing equilibrium isotope exchange may make a minor contribution to the observed direction of the fractionation (enrichment of the heavy isotope in the U^{IV} product, as demonstrated by Wang *et al.*, 2015), it does not account for the magnitude of isotope fractionation during the kinetic reaction of biological reduction.

To calculate the contribution of the NFSE and the mass effect to the fractionation factors obtained for each isotope during the enzymatic reduction, we used the methods of Fujii *et al.* (2009) and Moynier *et al.* (2009) to obtain the scaling factors of the conventional mass effect and the nuclear field shift term that appear in Bigeleisen's (1996) theory (Figs. 4, S-6). Whilst this analysis was developed initially for isotopic equilibrium conditions, it succeeds in reproducing the odd-even staggering trend (highlighted by the regression of the even isotopes in Fig. S-6) and suggests the dominant contribution of the NFSE to the overall observed kinetic fractionation factors.

Kinetic fractionations of U isotopes in the laboratory and nature consistently show lower fractionation than that predicted or measured at equilibrium (Fujii *et al.*, 2006; Abe *et al.*, 2008, 2010; Basu *et al.*, 2014; Wang *et al.*, 2015; Stirling *et al.*, 2015; Stylo *et al.*, 2015; Andersen *et al.*, 2017; Brown *et al.*, 2018; Sato *et al.*, 2021; Li and Tissot, 2023). However, the extent to which the relative contributions of the mass effect and the NFSE lead to this discrepancy has not been explored. This is of fundamental importance to the understanding of how isotope fractionation observed during kinetic reactions relates to that calculated for isotopic equilibrium. Thus, we compared the magnitudes of the decomposed mass and field shift effects from the experimental kinetic reaction (ε^{kin}), to the mass and field shift effect contributions determined for full equilibrium fractionation *via ab initio* calculations (ε^{eq}) (Fig. 4). This comparison reveals that the contribution of the mass effect to ε^{kin} approximates that predicted for equilibrium, no matter whether the tri- or dicarbonate U^{VI} species is assumed to be preferentially reduced by the bacterium (Fig. 4; trend (i)). On the other hand, the analysis indicates that the contribution of the NFSE to ε^{kin} is typically much smaller than that for ε^{eq}, but varies depending on the calculation method (density functional theory (DFT) *versus* Hartree-Fock (HF)) and the U^{VI} species used (Fig. 4a–c; trend (ii)). Indeed, calculations using DFT and the dicarbonate U^{VI} species appear to suggest that the isotope fractionation of the kinetic reaction approaches full equilibrium (Fig. 4d; trend (iii)). However, previous calculations using the HF method showed better agreement with the experimental ε^{eq} for the U^{VI}/U^{IV}-chloride isotope exchange reaction compared with DFT calculations, suggesting that the results of the HF method may be more accurate (Wang *et al.*, 2015; Sato *et al.*, 2021). Whilst *ab initio* calculations of ε^{eq} are not easy to verify due to a lack of experimental data with which to validate them, these data suggest that the mass effect has reached equilibrium, whilst the NFSE has not. This raises the question of how these two effects are manifested during kinetic reactions and what controls their relative expressions.

A recent study by Brown *et al.* (2018) explored the effect of abiotic U^{VI} reduction rates, controlled by U speciation, on attendant U isotope fractionation. To explain the inverse reaction rate-fractionation relationship, a model was developed incorporating a variable contribution of the NFSE that was dependent on the ratio of forward to backward reactions, but that also required isotopic exchange between U^{VI} and U^{IV}. However, in our study we observed only a minor contribution from equilibrium isotope exchange that cannot explain the magnitude of isotope fractionation during the kinetic reaction and this suggests that kinetic fractionation may also include the NFSE.

The mathematical basis for the inclusion of NFSE in kinetic fractionation has been derived by Sato *et al.* (2021). The authors introduced a model of kinetic uranium isotope fractionation that incorporates transition state theory to allow the inclusion of the NFSE within a multi-step U^{VI} reduction reaction, independent of subsequent equilibrium isotope exchange between the oxidised and reduced U. The model was then employed to re-interpret the data of Brown *et al.* (2018), demonstrating that the observations can arise from kinetic fractionation components that include the NFSE, without the requirement for independent equilibrium isotope exchange between the initial reactant and the final product. Rather, the model indicates that the magnitude of NFSE expression is dependent on the degree of reverse electron transfer (back reaction). This has since been confirmed experimentally using purified U^{VI} reducing proteins of various redox states. Fully reduced proteins facilitated rapid electron transfer with limited back reaction and little isotopic fractionation, whereas partially reduced proteins permitted significant NFSE-dominated fractionation linked to the allowance for extensive reverse electron transfer (Brown *et al.*, 2023).

Our data support the view that the mass effect is both an equilibrium and kinetic isotope fractionation, in which the full fractionation at equilibrium can be expressed during kinetically controlled reactions. On the other hand, the NFSE may be exclusively an equilibrium fractionation between the instantaneous products and transition state(s), and the transition state(s) and the reactants, and as such, its expression during kinetic fractionation within the reduction reaction may be dependent on reaction reversibility (Fujii *et al.*, 2009; Moynier *et al.*, 2013; Yang and Liu, 2016; Sato *et al.*, 2021). This would explain the range of fractionation factors observed in the laboratory and nature, including both mass-dependent and mass-independent directions of fractionation.

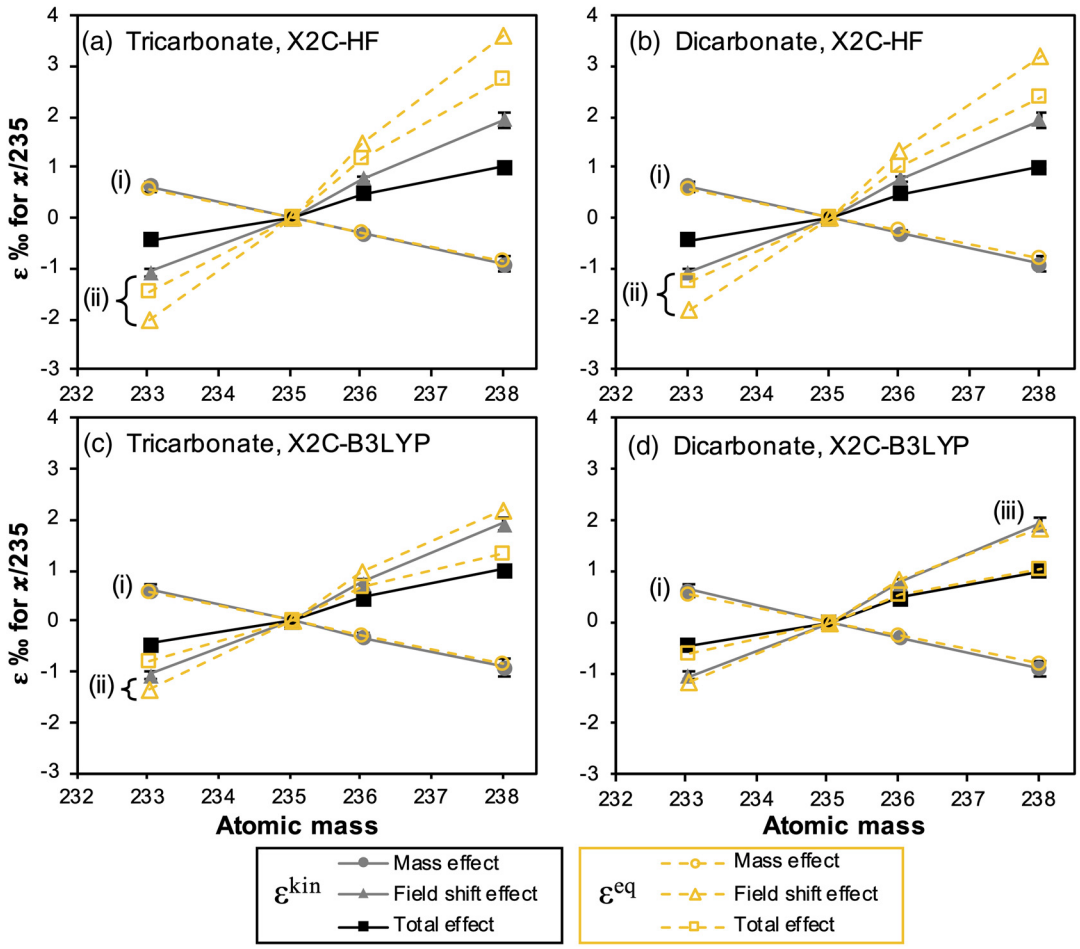

Figure 4 Isotope enrichment factors from the bacterial reduction experiment (ε^{kin}) and *ab initio* calculated equilibrium isotope enrichment factors (ε^{eq}) for the mass effect, the nuclear field shift effect and their sum (total effect) for each atomic mass. Equilibrium calculations were performed for either **(a, c)** tricarbonate, $UO_2(CO_3)_3^{4-}$, or **(b, d)** dicarbonate, $UO_2(CO_3)_2^{2-}$, as the U^{VI} species. Calculations of ln K_{nv} for ε^{eq} were performed using either **(a, b)** the Hartree-Fock method (X2C-HF) or **(c, d)** density functional theory (DFT) with the B3LYP functional (X2C-B3LYP). Symbols and error bars depict the mean and standard deviation of values derived from analysis of the data from duplicate reactors. A comparison of experimentally measured ε and recalculated total ε (after decomposition of the experimental data into the field shift and mass effect terms) is presented in Figure S-6. Trend (i) points to the consistent values obtained for MDF from theory and experiment, (ii) points to the discrepancy between theory and experiment for the NFSE contribution in three of the four cases, and (iii) points to the agreement between NFSE theory and experiment in the case of dicarbonate speciation and DFT calculations.

Further work is required to explore the factors that control the relative contributions of the two effects during kinetic isotope fractionations and rule out the contribution of other isotope effects, *e.g.*, a nuclear spin effect or magnetic isotope effect (Epov *et al.*, 2011). Indeed, different reaction mechanisms of Hg reduction, *e.g.*, photoreduction *versus* reduction by dissolved organic matter or $SnCl_2$, resulted in different relative contributions of mass-dependent and mass-independent fractionation (Bergquist and Blum, 2007; Zheng and Hintelmann, 2010).

Collectively, the data presented here show unambiguous evidence for the contribution of the nuclear field shift to isotope fractionation during kinetic U reduction and confirm that previously observed fractionations (reporting enrichment of the heavy isotope in the product) arise from the dominance of the nuclear field shift effect.

Acknowledgements

Funding for this work was provided by an ERC consolidator grant awarded to RB-L (725675: UNEARTH: "Uranium isotope fractionation: a novel biosignature to identify microbial metabolism on early Earth"). This work was also supported by JSPS KAKENHI Grant Numbers JP19K22171, JP21H01864 and JP22J12551. A part of the calculations was performed at the Research Center for Computational Science, Okazaki, Japan (Project: 21-IMS-C049 and 22-IMS-C049).

Editor: Claudine Stirling

Additional Information

Supplementary Information accompanies this letter at https://www.geochemicalperspectivesletters.org/article2333.

Cite this letter as: Brown, A.R., Roebbert, Y., Sato, A., Hada, M., Abe, M., Weyer, S., Bernier-Latmani, R. (2023) Contribution of the nuclear field shift to kinetic uranium isotope fractionation. *Geochem. Persp. Let.* 27, 43–47. https://doi.org/10.7185/geochemlet.2333

References

Abe, M., Suzuki, T., Fujii, Y., Hada, M., Hirao, K. (2008) An *ab initio* molecular orbital study of the nuclear volume effects in uranium isotope fractionations. *The Journal of Chemical Physics* 129, 164309. https://doi.org/10.1063/1.2992616

Abe, M., Suzuki, T., Fujii, Y., Hada, M., Hirao, K. (2010) Ligand effect on uranium isotope fractionations caused by nuclear volume effects: An *ab initio* relativistic molecular orbital study. *The Journal of Chemical Physics* 133, 044309. https://doi.org/10.1063/1.3463797

Andersen, M.B., Stirling, C.H., Weyer, S. (2017) Uranium Isotope Fractionation. *Reviews in Mineralogy and Geochemistry* 82, 799–850. https://doi.org/10.2138/rmg.2017.82.19

Angeli, I., Marinova, K.P. (2013) Table of experimental nuclear ground state charge radii: An update. *Atomic Data and Nuclear Data Tables* 99, 69–95. https://doi.org/10.1016/j.adt.2011.12.006

Basu, A., Sanford, R.A., Johnson, T.M., Lundstrom, C.C., Löffler, F.E. (2014) Uranium isotopic fractionation factors during U(VI) reduction by bacterial isolates. *Geochimica et Cosmochimica Acta* 136, 100–113. https://doi.org/10.1016/j.gca.2014.02.041

Basu, A., Wanner, C., Johnson, T.M., Lundstrom, C.C., Sanford, R.A., Sonnenthal, E.L., Boyanov, M.I., Kemner, K.M. (2020) Microbial U Isotope Fractionation Depends on the U(VI) Reduction Rate. *Environmental Science & Technology* 54, 2295–2303. https://doi.org/10.1021/acs.est.9b05935

Bergquist, B.A., Blum, J.D. (2007) Mass-Dependent and -Independent Fractionation of Hg Isotopes by Photoreduction in Aquatic Systems. *Science* 318, 417–420. https://doi.org/10.1126/science.1148050

Bigeleisen, J. (1996) Nuclear Size and Shape Effects in Chemical Reactions. Isotope Chemistry of the Heavy Elements. *Journal of the American Chemical Society* 118, 3676–3680. https://doi.org/10.1021/ja954076k

Bopp IV, C.J., Lundstrom, C.C., Johnson, T.M., Sandford, R.A., Long, P.E., Williams, K.H. (2010) Uranium $^{238}U/^{235}U$ Isotope Ratios as Indicators of Reduction: Results from an in situ Biostimulation Experiment at Rifle, Colorado, U.S.A. *Environmental Science & Technology* 44, 5927–5933. https://doi.org/10.1021/es100643v

Brown, A.R., Molinas, M., Roebbert, Y., Sato, A., Abe, M., Weyer, S., Bernier-Latmani, R. (2023) Electron flux is a key determinant of uranium isotope fractionation during bacterial reduction. *Communications Earth & Environment* 4, 329. https://doi.org/10.1038/s43247-023-00989-x

Brown, S.T., Basu, A., Ding, X., Christensen, J.N., DePaolo, D.J. (2018) Uranium isotope fractionation by abiotic reductive precipitation. *Proceedings of the National Academy of Sciences* 115, 8688–8693. https://doi.org/10.1073/pnas.1805234115

Epov, V.N., Malinovskiy, D., Vanhaecke, F., Bégué, D., Donard, O.F.X. (2011) Modern mass spectrometry for studying mass-independent fractionation of heavy stable isotopes in environmental and biological sciences. *Journal of Analytical Atomic Spectrometry* 26, 1142–1156. https://doi.org/10.1039/c0ja00231c

Fujii, T., Moynier, F., Albarède, F. (2009) The nuclear field shift effect in chemical exchange reactions. *Chemical Geology* 267, 139–156. https://doi.org/10.1016/j.chemgeo.2009.06.015

Fujii, Y., Nomura, M., Okamoto, M., Onitsuka, H., Kawakami, F., Takeda, K. (1989a) An Anomalous Isotope Effect of ^{235}U in U(IV)-U(VI) Chemical Exchange. *Zeitschrift für Naturforschung A* 44, 395–398. https://doi.org/10.1515/zna-1989-0507

Fujii, Y., Nomura, M., Onitsuka, H., Takeda, K. (1989b) Anomalous Isotope Fractionation in Uranium Enrichment Process. *Journal of Nuclear Science and Technology* 26, 1061–1064. https://doi.org/10.1080/18811248.1989.9734427

Fujii, Y., Higuchi, N., Haruno, Y., Nomura, M., Suzuki, T. (2006) Temperature Dependence of Isotope Effects in Uranium Chemical Exchange Reactions. *Journal of Nuclear Science and Technology* 43, 400–406. https://doi.org/10.1080/18811248.2006.9711111

Kritee, K., Barkay, T., Blum, J.D. (2009) Mass dependent stable isotope fractionation of mercury during *mer* mediated microbial degradation of monomethylmercury. *Geochimica et Cosmochimica Acta* 73, 1285–1296. https://doi.org/10.1016/j.gca.2008.11.038

Li, H., Tissot, F.L.H. (2023) UID: The uranium isotope database. *Chemical Geology* 618, 121221. https://doi.org/10.1016/j.chemgeo.2022.121221

Moynier, F., Fujii, T., Telouk, P. (2009) Mass-independent isotopic fractionation of tin in chemical exchange reaction using a crown ether. *Analytica Chimica Acta* 632, 234–239. https://doi.org/10.1016/j.aca.2008.11.015

Moynier, F., Fujii, T., Brennecka, G.A., Nielsen, S.G. (2013) Nuclear field shift in natural environments. *Comptes Rendus Geoscience* 345, 150–159. https://doi.org/10.1016/j.crte.2013.01.004

Nomura, M., Higuchi, N., Fujii, Y. (1996) Mass Dependence of Uranium Isotope Effects in the U(IV)−U(VI) Exchange Reaction. *Journal of the American Chemical Society* 118, 9127–9130. https://doi.org/10.1021/ja954075s

Sato, A., Bernier-Latmani, R., Hada, M., Abe, M. (2021) Ab initio and steady-state models for uranium isotope fractionation in multi-step biotic and abiotic reduction. *Geochimica et Cosmochimica Acta* 307, 212–227. https://doi.org/10.1016/j.gca.2021.05.044

Schauble, E.A. (2007) Role of nuclear volume in driving equilibrium stable isotope fractionation of mercury, thallium, and other very heavy elements. *Geochimica et Cosmochimica Acta* 71, 2170–2189. https://doi.org/10.1016/j.gca.2007.02.004

Stirling, C.H., Andersen, M.B., Warthmann, R., Halliday, A.N. (2015) Isotope fractionation of ^{238}U and ^{235}U during biologically-mediated uranium reduction. *Geochimica et Cosmochimica Acta* 163, 200–218. https://doi.org/10.1016/j.gca.2015.03.017

Stylo, M., Neubert, N., Wang, Y., Monga, N., Romaniello, S.J., Weyer, S., Bernier-Latmani, R. (2015) Uranium isotopes fingerprint biotic reduction. *Proceedings of the National Academy of Sciences* 112, 5619–5624. https://doi.org/10.1073/pnas.1421841112

Wall, J.D., Krumholz, L.R. (2006) Uranium Reduction. *Annual Review of Microbiology* 60, 149–166. https://doi.org/10.1146/annurev.micro.59.030804.121357

Wang, X., Johnson, T.M., Lundstrom, C.C. (2015) Low temperature equilibrium isotope fractionation and isotope exchange kinetics between U(IV) and U(VI). *Geochimica et Cosmochimica Acta* 158, 262–275. https://doi.org/10.1016/j.gca.2015.03.006

Yang, S., Liu, Y. (2016) Nuclear field shift effects on stable isotope fractionation: a review. *Acta Geochimica* 35, 227–239. https://doi.org/10.1007/s11631-016-0109-3

Zheng, W., Hintelmann, H. (2010) Nuclear Field Shift Effect in Isotope Fractionation of Mercury during Abiotic Reduction in the Absence of Light. *The Journal of Physical Chemistry A* 114, 4238–4245. https://doi.org/10.1021/jp910353y

Geochemical Perspectives Letters

Contribution of the nuclear field shift to kinetic uranium isotope fractionation

A.R. Brown, Y. Roebbert, A. Sato, M. Hada, M. Abe, S. Weyer, R. Bernier-Latmani

Supplementary Information

The Supplementary Information includes:

- Experimental Section
- Table S-1
- Figures S-1 to S-6
- Supplementary Information References

Experimental Section

Preparation of the U multi-isotope standard

The ^{233}U, ^{235}U, ^{236}U, ^{238}U standard was prepared by mixing the reference materials IRMM-184 (natural U) and IRMM-3636 (a 1:1 mix of the ^{233}U and ^{236}U 'double spike') at an approximate ratio of 25:1 to give a $^{236/233}U/^{235}U$ ratio of ~3. The nitric acid matrix was then evaporated and replaced with 6 N ultra-pure HCl, followed by evaporation and replacement with 0.1 N ultra-pure HCl. The standard was then moved to an anoxic chamber (100 % N_2, <0.1 ppm O_2; MBraun, Germany).

Culturing of *Shewanella oneidensis*

Shewanella oneidensis MR-1 was grown in oxic Luria-Bertani (LB) medium to mid-late exponential phase. Cultures were then harvested by centrifugation for 10 min at 5000 × *g* and washed three times in a sterile anoxic buffer containing 30 mM sodium bicarbonate and 20 mM piperazine-N,N′-bis(2-ethanesulfonic acid) (PIPES) at pH 7.3. Finally, the cultures were resuspended in the same medium to an appropriate density, prior to addition to experimental reactors.

Reduction of U^{VI} by *S. oneidensis*

Anoxic reactors containing 30 mM sodium bicarbonate and 20 mM PIPES at pH 7.3 were prepared. 20 mM sodium lactate was supplied as the electron donor. All experimental media were autoclaved, flushed with pure and sterile N_2 for several hours and then stored in the dark at ~25 °C inside an anoxic chamber. 200 µM of the U^{VI} multi-isotope standard was added from an anoxic ~20 mM U chloride stock. Aliquots of the anoxic *S. oneidensis* cell suspensions were then

added to the reactors to give a final optical density of 1, as measured at 600 nm (OD_{600nm}) using a UV-vis spectrophotometer, which was equivalent to approximately 5×10^8 cells mL^{-1}. Periodically, samples were removed for the analysis of aqueous U^{VI} concentrations and isotope ratio analysis. Approximately 0.5 mL was removed using a sterile, anoxic syringe and needle, and the sample was filtered through a 0.22 µm PTFE filter. This process removes both the solid phase U^{IV} and bacterial cells and thus, prevents any further reduction. Samples were then stored at −20 °C.

U isotope ratio analysis

Samples were first weighed and evaporated to dryness. The samples were treated with a mixture of 200 µl 14 M HNO_3 and 200 µl H_2O_2 (30 %) to destroy organic materials. Uranium was then purified by ion-exchange chromatography according to a method described by Weyer *et al.* (2008). The samples were dissolved in 1 mL 3 M HNO_3 and U was purified on Eichrom UTEVA resin.

U isotope measurements were performed at Leibniz Universität Hannover with a Thermo-Finnigan Neptune multi-collector ICP-MS (MC-ICP-MS), similar to the protocol published by Noordman *et al.* (2015). For sample introduction, a Cetac Aridus-II desolvation system equipped with a perfluoroalkoxy alkane (PFA) nebuliser with a sampling rate of 100 µL/min was used to enhance sensitivity and to reduce solvent-based interferences such as oxides and hydrides. Additionally, a standard Ni sampling cone and a Ni X skimmer cone were used in combination with a 0.8 mm copper ring (spacer). With this setup, a 210 ng/g solution achieved a signal of between 130 and 200 V on ^{238}U in low mass resolution mode.

The abundance sensitivity was determined before each analysis term and was typically ≤0.1 ppm of the ^{238}U signal at mass 236 (determined on a spike-free solution), resulting in negligible tail correction.

All samples and standards were measured with 320 s total integration time (80 cycles at 4 s integration time). A standard sample bracketing method was applied during analysis, *i.e.* one sample measurement was bracketed by two standard measurements. The results for all sample analyses are presented in the delta notation with respect to ^{235}U and relative to the U standard, *e.g.*, for ^{238}U:

$$\delta^{238}\mathrm{U}\ [‰] = \left[\frac{(^{238}\mathrm{U}/^{235}\mathrm{U})_{\mathrm{sample}}}{(^{238}\mathrm{U}/^{235}\mathrm{U})_{\mathrm{standard}}} - 1\right] \cdot 1000. \qquad \text{(Eq. S-1)}$$

Each sample was analysed three times and the precision is given as two standard deviations (2 s.d.) of the replicate analysis for each sample (with an average error of 0.19 ‰ for $\delta^{238}U$). Additionally, reproducibility and accuracy was determined by replicate analyses of the U-standards IRMM-184 (−1.17 ‰ ± 0.05) and REIMEP 18-A (−0.28 ‰ ± 0.07) relative to CRM-112A during each analysis session and the results agreed with those previously reported in the literature, within uncertainties (Weyer *et al.*, 2008; Richter *et al.*, 2010; Brennecka *et al.*, 2011; Noordmann *et al.*, 2015; Li and Tissot, 2023).

Rayleigh distillation models

Isotope fractionation factors were determined by fitting Rayleigh distillation models to the measured isotopic signatures, according to the method described in Scott *et al.* (2004) and using the following formula:

$$\delta_t = (\delta_0 + 1000\ ‰)\left[\frac{c_t}{c_0}\right]^{\alpha-1} - 1000\ ‰, \qquad \text{(Eq. S-2)}$$

where c_0 and δ_0 are the initial concentration and isotopic composition of U^{VI}, and c_t and δ_t are the concentration and isotopic composition of U^{VI} at time t. The fractionation factors (ε) were obtained from the slope ($\alpha - 1$) of the linear regression of the experimental data in linearised plots of $\ln(\delta^{238}U + 1000\ ‰)$ *versus* $\ln(c_t/c_0)$, where $\varepsilon = (\alpha - 1) \times 1000$.

Decomposition of ε

To calculate the contribution of the nuclear field shift effect (NFSE) and the mass effect to the fractionation factors obtained for each isotope during the enzymatic reduction, we used the methods of Fujii *et al.* (2009) and Moynier *et al.* (2009) to obtain the scaling factors of the conventional mass effect and the nuclear field shift term that appear in Bigeleisen's (1996) equation:

$$\ln \alpha = \left(\frac{hc}{kT}\right) f_s \times A + \frac{1}{24}\left(\frac{\hbar}{kT}\right)^2 \frac{\delta m}{mm'} \times B, \qquad \text{(Eq. S-3)}$$

where f_s is the field shift frequency, h is the Planck constant, c is the speed of light in a vacuum, k is the Boltzmann constant, T is temperature and $\hbar$ is the reduced Planck constant; m and m' are the masses of the heavy and light isotopes and δm equates to the mass difference, $m - m'$. Here, A is the scaling factor for the nuclear field shift effect (the first term on the right-hand side of Eq. S-3) and B is the scaling factor of the mass-dependent vibrational effect. We modified the mass-dependent fractionation term for the kinetic effect according to Zheng and Hintelmann (2010) after Young *et al.* (2002). As the field shift frequency is proportional to the mean-squared nuclear charge radius ($\delta\langle r^2\rangle_{235,i} = \delta\langle r^2\rangle_i - \delta\langle r^2\rangle_{235}$) (Bigeleisen, 1996), at constant temperature, Equation S-3 can be simplified to:

$$\ln \alpha = \delta\langle r^2\rangle \times a + \ln\left(\frac{m_{235}}{m_i}\right) \times b, \qquad \text{(Eq. S-4)}$$

where a and b are new scaling factors. Equation S-4 can then be linearised by rearrangement to give:

$$\frac{\varepsilon_i}{\ln(m_{235}/m_i)} = \frac{\delta\langle r^2\rangle_{235,i}}{\ln(m_{235}/m_i)} \times a + b. \qquad \text{(Eq. S-5)}$$

The scaling factors were then obtained from linear plots of the above parameters. The fractionation factors, ε (≈ ln α), for each isotope of mass m_i, with respect to ^{235}U (m_{235}), were obtained from the Rayleigh distillation models. Mean square nuclear charge radii ($\delta\langle r^2\rangle_{235,i} = \delta\langle r^2\rangle_i - \delta\langle r^2\rangle_{235}$) for each atomic mass were taken from Angeli and Marinova (2013). The contributions of the nuclear field shift term and the mass term to the overall observed fractionation factor were then calculated using Equation S-4.

***Ab initio* calculation of ε^{eq} between U^{VI} and U^{IV}**

We modelled the tri- and di-carbonate complexes, *i.e.* $UO_2(CO_3)_3^{4-}$ and $UO_2(CO_3)_2^{2-}$, as the U^{VI} species because they are the dominant U^{VI} species under our experimental conditions (Fig. S1). The dominant product of U^{VI} reduction by *S. oneidensis* MR-1 under these same conditions is a non-uraninite U^{IV} (Stylo *et al.*, 2015). As ningyoite ($CaU(PO_4)_2$) is a close analogue of these non-crystalline biotic reduction products (Bernier-Latmani *et al.*, 2010; Alessi *et al.*, 2014; Sato *et al.*, 2021), we modelled the U^{IV} as a cluster of ningyoite ($H_{26}CaU(PO_4)_{10}^{2+}$), as established previously (Sato *et al.*, 2021).

ε^{eq} was calculated as the sum of the nuclear mass term, ln K_{nm} (Bigeleisen and Mayer, 1947), and the NFSE term, ln K_{fs} (Bigeleisen, 1996; Nomura *et al.*, 1996; Fujii *et al.*, 2009), at a temperature of 298 K, the same as the microbial U^{VI} reduction experiments:

$$\varepsilon^{eq} = \ln K_{nm} + \ln K_{fs}. \qquad \text{(Eq. S-6)}$$

The nuclear mass term, ln K_{nm}, was calculated as a difference in the logarithms of the reduced partition function ratio, β, of U^{IV} and U^{VI}:

$$\ln K_{\mathrm{nm}} = \ln \beta\left(\mathrm{U^{IV}}\right) - \ln \beta\left(\mathrm{U^{VI}}\right) \quad , \qquad \text{(Eq. S-7)}$$

where, ln β is described by the harmonic frequencies, ν:

$$\ln \beta = \ln\left[\prod_i \frac{u_i}{u_i'} \frac{e^{-u_i/2}/(1-e^{-u_i})}{e^{-u_i'/2}/\left(1-e^{-u_i'}\right)}\right],\ u_i \equiv \frac{h\nu_i}{k_{\mathrm{B}}T}. \qquad \text{(Eq. S-8)}$$

Here, h is the Planck constant, k_{B} is the Boltzmann constant and T is the absolute temperature. The indices of the vibrational modes are denoted by the subscript i, and the quantities for the light isotope are indicated by the prime notation.

The NFSE term, ln K_{fs}, was calculated from the ground-state electronic energies of isotopologues of $\mathrm{U^{VI}}$ and $\mathrm{U^{IV}}$:

$$\ln K_{\mathrm{fs}} = \left[\left\{E\left(^{238}\mathrm{U^{VI}}\right) - E\left(^{235}\mathrm{U^{VI}}\right)\right\} - \left\{E\left(^{238}\mathrm{U^{IV}}\right) - E\left(^{235}\mathrm{U^{IV}}\right)\right\}\right]/k_{\mathrm{B}}T \quad . \qquad \text{(Eq. S-9)}$$

The geometry optimisation and the vibrational analysis for the calculation of ln K_{nm} were conducted with the Gaussian 09 software package (Frisch *et al.*, 2009). These calculations used density functional theory (DFT) with the hybrid exchange-correlation functional consisting of Becke's (1993) three-parameter non-local hybrid exchange potential with Lee-Yang-Parr non-local functionals (B3LYP) (Lee *et al.*, 1988; Stephens *et al.*, 1994). We used Stuttgart-type small core relativistic pseudopotentials named ECP60MWB (Küchle *et al.*, 1994) with a contracted Gaussian basis set of [10s, 9p, 5d, 5f, 3g] (Cao and Dolg, 2004) for U and the 6-31+G(d) basis set for the remaining atoms. The solvation effects were modelled by using the polarisable continuum model (Scalmani and Frisch, 2010) assuming the water solvent condition, *i.e.* a dielectric constant of 78.39.

Vibrational frequencies for the ^{233}U isotopologue could not be calculated because the mass data for ^{233}U is not supported in Gaussian 09. Therefore, ln β for ^{233}U/^{235}U was estimated by extrapolating the data from ln β for ^{234}U/^{235}U, ^{236}U/^{235}U, and ^{238}U/^{235}U using the proportional relationship between ln β and mass.

For the optimised ground-state geometry, we performed the electronic energy calculations with DIRAC16 software package (Jensen *et al.*, 2016; Saue *et al.*, 2020) at the Hartree-Fock (HF) and DFT levels with the exact two-component (X2C) relativistic Hamiltonian (Iliaš and Saue, 2007; Liu, 2010; Saue, 2011; Knecht *et al.*, 2022) to calculate ln K_{fs}. In the X2C-DFT calculations, we used the B3LYP hybrid exchange-correlation functional (Lee *et al.*, 1988; Becke, 1993; Stephens *et al.*, 1994). We used the Dyall.cv2z basis set (Dyall, 2007) for U and the 6-31+G(d) basis set for the remaining atoms.

To model the nuclear volume of each isotope, we used the Gaussian-type finite nucleus model (Visscher and Dyall, 1997) with the experimentally determined root-mean-square nuclear charge radii of ^{233}U, ^{235}U, ^{236}U, and ^{238}U which are 5.8203 fm, 5.8337 fm, 5.8431 fm, and 5.8571 fm, respectively (Angeli and Marinova, 2013).

For each molecular model, we optimised only the wave functions of ^{238}U isotopologue and used them to calculate the electronic energies of other isotopologues. This strategy is based on the demonstration of the previous studies that the effect of the optimisation for a single isotope is minor (Fricke and Waber, 1972; Filatov, 2007; Knecht *et al.*, 2011) and may suppress the unphysical numerical errors caused by the optimisation of the wave functions of all the isotopologues (Sato *et al.*, 2021).

Supplementary Table

Table S-1 ln K_{fs} (nuclear field shift effect term), ln K_{nm} (nuclear mass term) and ε^{eq} (total fractionation factor) for the reduction of the two dominant species of U^{VI}-carbonate to U^{IV}. ln K_{fs} was calculated by either X2C-Hartree-Fock (X2C-HF) or X2C-B3LYP, and the values are shown in the columns of "HF" and "B3LYP", respectively. Likewise, the total fractionation factor is shown for both calculation methods of ln K_{fs}. All values are shown in units of ‰ (permil). The computational methods are described above.

Reaction	Isotope pair	ln K_{fs}		ln K_{nm}	ε^{eq}	
		HF	B3LYP		HF	B3LYP
$U^{VI}O_2(CO_3)_3^{4-} \longrightarrow CaU^{IV}(PO_4)_2$	233/235	−2.03	−1.36	0.58	−1.45	−0.78
	236/235	1.47	0.97	−0.29	1.18	0.68
	238/235	3.57	2.21	−0.86	2.71	1.34
$U^{VI}O_2(CO_3)_2^{2-} \longrightarrow CaU^{IV}(PO_4)_2$	233/235	−1.83	−1.17	0.55	−1.28	−0.62
	236/235	1.31	0.83	−0.27	1.04	0.56
	238/235	3.21	1.87	−0.81	2.39	1.06

Supplementary Figures

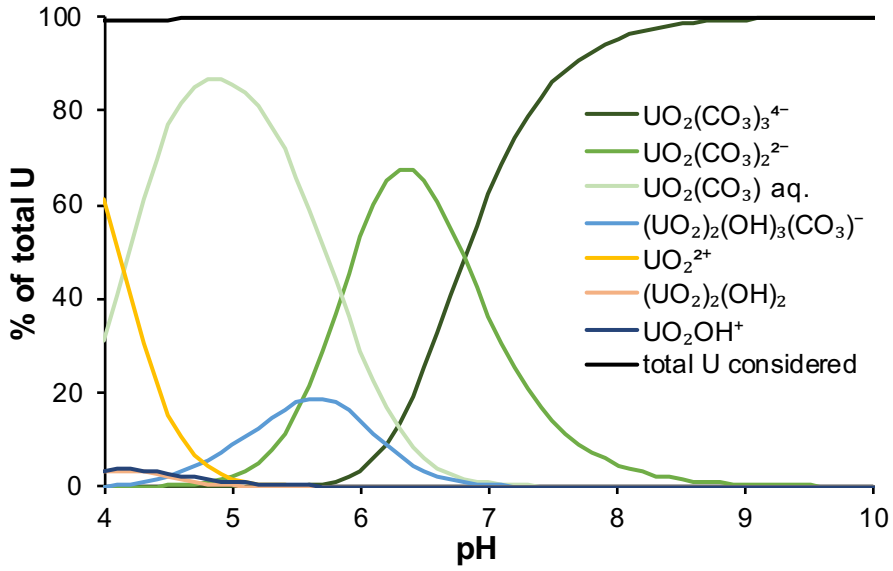

Figure S-1 Aqueous U speciation as a function of pH in systems containing 200 µM U and 30 mM sodium bicarbonate at 25 °C. Calculations were performed using MINEQL+ v5 using updated formation constants for uranium carbonate complexes (Guillaumont *et al.*, 2003; Hummel *et al.*, 2005). Below pH ~5.5, only U species contributing >0.5 % of the total U have been included in the plot in order to simplify visualisation.

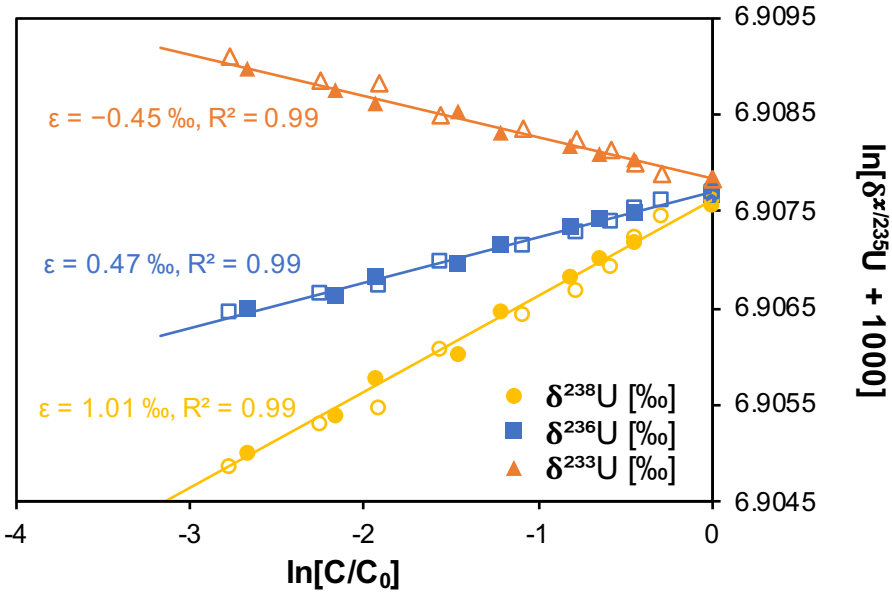

Figure S-2 Linearised plots of $\delta^{x/235}$U isotope signatures, as a function of reaction progression. Filled and open symbols depict duplicate reactors. Linear regressions represent Rayleigh distillation models and their corresponding isotope enrichment factors (ε) and R^2 values for the mean of duplicate reactors.

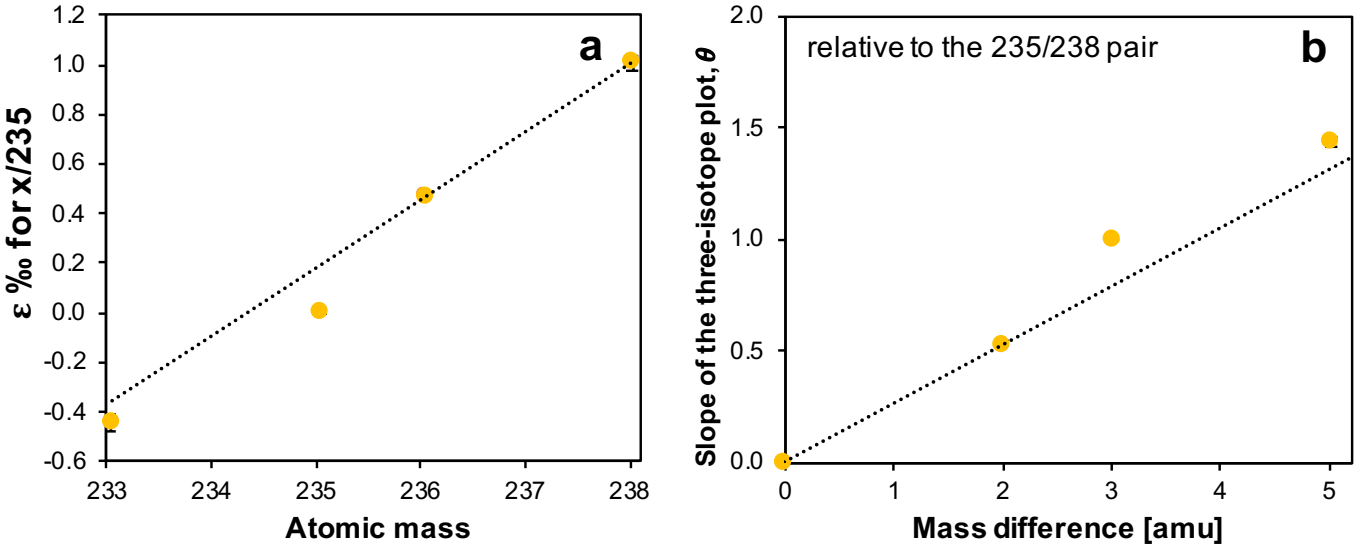

Figure S-3 **(a)** Fractionation factors (ε) for each atomic mass. Symbols and error bars depict the mean and standard deviation of duplicate reactors. Where not visible, the error is within the size of the symbol. The dotted line represents the linear regression of the even isotopes only. **(b)** Slopes of the three-isotope plots, θ, relative to the $^{235}U/^{238}U$ pair. Slopes were calculated according to Nomura *et al.* (1996) and defined as follows: $\theta = \ln \beta_{(j/238)} / \ln \beta_{(235/238)}$, where j = 233, 235, 236 or 238 and $\beta_{(j/238)} = r_{(j/238),i} / r_{(j/238),0}$. Here, r represents the isotopic ratio for the respective isotope pairs for a given sample (i) or the starting material (0). The mass difference of 0 = ^{238}U, 2 = ^{236}U, 3 = ^{235}U and 5 = ^{233}U. The dotted line represents the linear regression of the even isotopes only.

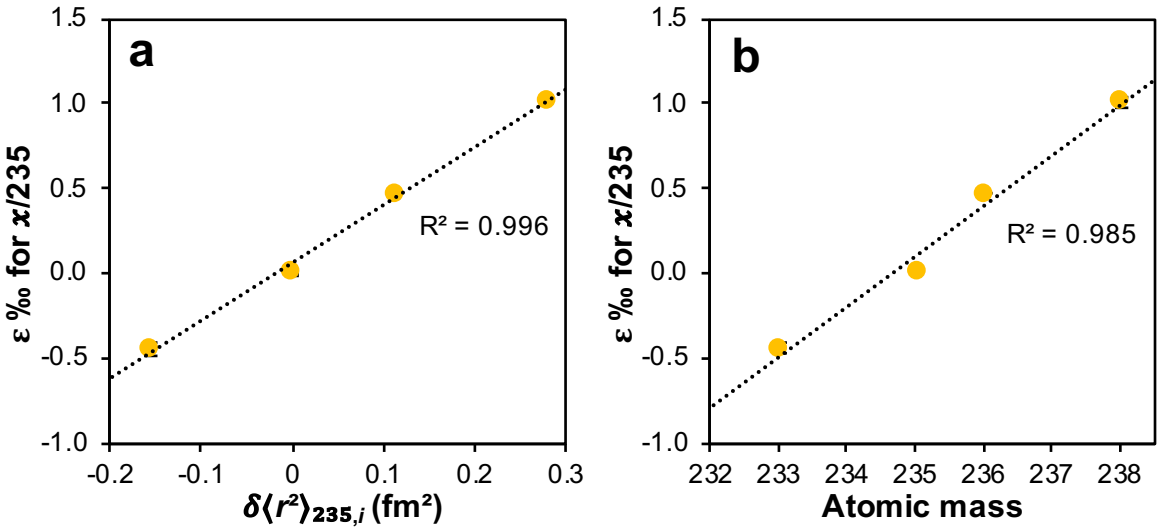

Figure S-4 **(a)** Fractionation factors (ε) for the mean square nuclear charge radii of each isotope ($\delta\langle r^2\rangle_{235,i} = \delta\langle r^2\rangle_i - \delta\langle r^2\rangle_{235}$). Symbols and error bars depict the mean and standard deviation of duplicate reactors. Where not visible, the error is within the size of the symbol. Mean square nuclear charge radii for each atomic mass were taken from Angeli and Marinova (2013). **(b)** Fractionation factors (ε) for each atomic mass. Symbols and error bars depict the mean and standard deviation of duplicate reactors. Where not visible, the error is within the size of the symbol.

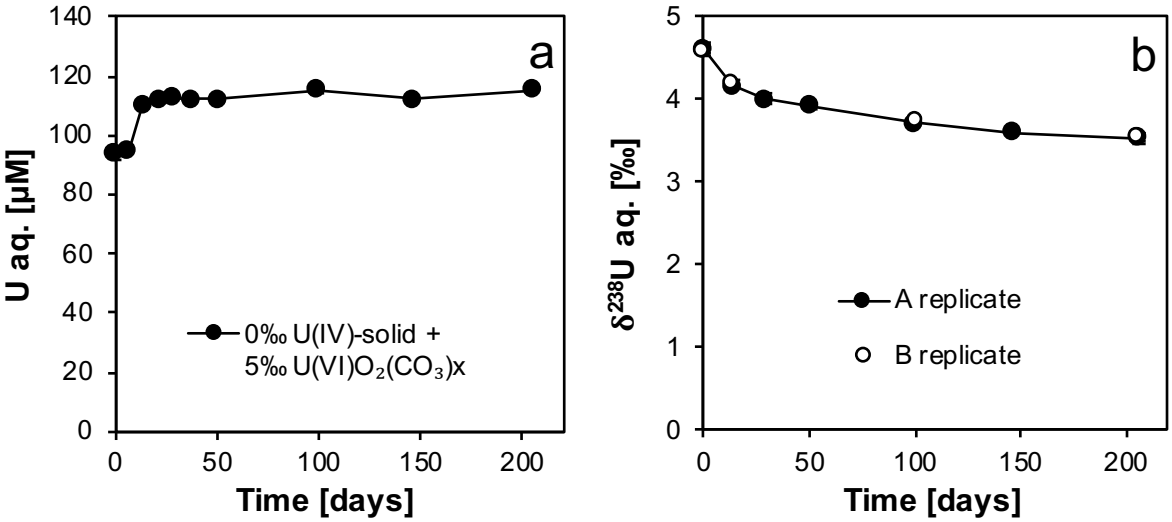

Figure S-5 **(a)** Aqueous uranium concentrations during equilibrium isotope exchange experiments between ~100 µM aqueous U^{VI}-carbonate (30 mM sodium bicarbonate) with an initial isotopic composition of ~5 ‰ and ~43 µM of solid U^{IV} product of the bioreduction experiments with an initial isotopic composition of 0 ‰. Samples were filtered through 0.22 µm filters. Symbols and error bars depict 1 standard deviation of the mean of duplicate reactors. Where not visible, the error is smaller than the symbol size. **(b)** $\delta^{238}U$ values of the aqueous U over time. Symbols and error bars depict 2 standard deviations of the mean of triplicate measurements.

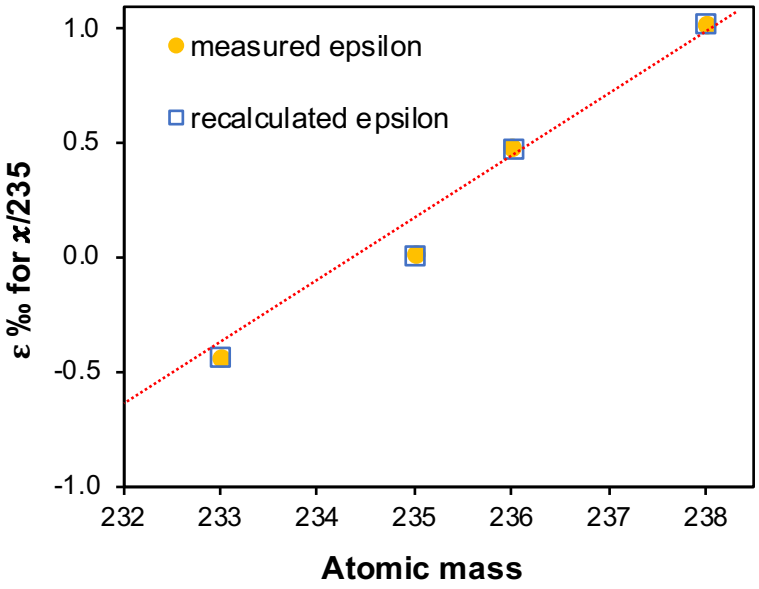

Figure S-6 Isotope enrichment factors, ε, for each atomic mass with respect to ^{235}U. Recalculated values represent the sum of the extracted mass and nuclear volume terms, determined by the methods described by Fujii *et al.* (2009) and Moynier *et al.* (2009), after Bigeleisen (1996). The dotted red line represents the linear regression of the recalculated values of the even isotopes only and indicates the presence of the odd-even staggering trend (deviation from mass dependence).

Supplementary Information References

Alessi, D.S., Lezama-Pacheco, J.S., Stubbs, J.E., Janousch, M., Bargar, J.R., Persson, P., Bernier-Latmani, R. (2014) The product of microbial uranium reduction includes multiple species with U(IV)-phosphate coordination. *Geochimica et Cosmochimica Acta* 131, 115–127. https://doi.org/10.1016/j.gca.2014.01.005

Angeli, I., Marinova, K.P. (2013) Table of experimental nuclear ground state charge radii: An update. *Atomic Data and Nuclear Data Tables* 99, 69–95. https://doi.org/10.1016/j.adt.2011.12.006

Becke, A.D. (1993) Density-functional thermochemistry. III. The role of exact exchange. *The Journal of Chemical Physics* 98, 5648–5652. https://doi.org/10.1063/1.464913

Bernier-Latmani, R., Veeramani, H., Vecchia, E.D., Junier, P., Lezama-Pacheco, J.S., Suvorova, E.I., Sharp, J.O., Wigginton, N.S., Bargar, J.R. (2010) Non-uraninite Products of Microbial U(VI) Reduction. *Environmental Science & Technology* 44, 9456–9462. https://doi.org/10.1021/es101675a

Bigeleisen, J. (1996) Nuclear Size and Shape Effects in Chemical Reactions. Isotope Chemistry of the Heavy Elements. *Journal of the American Chemical Society* 118, 3676–3680. https://doi.org/10.1021/ja954076k

Bigeleisen, J., Mayer, M.G. (1947) Calculation of Equilibrium Constants for Isotopic Exchange Reactions. *The Journal of Chemical Physics* 15, 261–267. https://doi.org/10.1063/1.1746492

Brennecka, G.A., Wasylenki, L.E., Bargar, J.R., Weyer, S., Anbar, A.D. (2011) Uranium Isotope Fractionation during Adsorption to Mn-Oxyhydroxides. *Environmental Science & Technology* 45, 1370–1375. https://doi.org/10.1021/es103061v

Cao, X., Dolg, M. (2004) Segmented contraction scheme for small-core actinide pseudopotential basis sets. *Journal of Molecular Structure: THEOCHEM* 673, 203–209. https://doi.org/10.1016/j.theochem.2003.12.015

Dyall, K.G. (2007) Relativistic double-zeta, triple-zeta, and quadruple-zeta basis sets for the actinides Ac–Lr. *Theoretical Chemistry Accounts* 117, 491–500. https://doi.org/10.1007/s00214-006-0175-4

Filatov, M. (2007) On the calculation of Mössbauer isomer shift. *The Journal of Chemical Physics* 127, 084101. https://doi.org/10.1063/1.2761879

Fricke, B., Waber, J.T. (1972) Calculation of Isomer Shift in Mössbauer Spectroscopy. *Physical Review B* 5, 3445–3449. https://doi.org/10.1103/PhysRevB.5.3445

Frisch, M.J., Trucks, G.W., Schlegel, H.B., Scuseria, G.E., Robb, M.A., *et al*. (2009) *Gaussian 09, Revision C.01*. Gaussian, Inc., Wallingford, CT. https://gaussian.com/g09_c01/

Fujii, T., Moynier, F., Albarède, F. (2009) The nuclear field shift effect in chemical exchange reactions. *Chemical Geology* 267, 139–156. https://doi.org/10.1016/j.chemgeo.2009.06.015

Guillaumont, R., Fanghänel, T., Fuger, J., Grenthe, I., Neck, V., Palmer, D.A., Rand, M.H. (2003) *Update on the Chemical Thermodynamics of Uranium, Neptunium, Plutonium, Americium and Technetium*. OECD Nuclear Energy Agency, Issy-les-Moulineaux, and Elsevier, Amsterdam.

Hummel, W., Anderegg, G., Puigdomènech, I., Rao, L., Tochiyama, O. (2005) *Chemical Thermodynamics of Compounds and Complexes of U, Np, Pu, Am, Tc, Se, Ni and Zr with Selected Organic Ligands*. OECD Nuclear Energry Agency, Issy-les-Moulineaux, and Elsevier, Amsterdam.

Iliaš, M., Saue, T. (2007) An infinite-order two-component relativistic Hamiltonian by a simple one-step transformation. *The Journal of Chemical Physics* 126, 064102. https://doi.org/10.1063/1.2436882

Jensen, H.J.A., Bast, R., Saue, T., Visscher, L., Bakken, V., *et al*. (2016) DIRAC, a relativistic *ab initio* electronic structure program, Release DIRAC16. http://www.diracprogram.org/

Knecht, S., Fux, S., van Meer, R., Visscher, L., Reiher, M., Saue, T. (2011) Mössbauer spectroscopy for heavy elements: a relativistic benchmark study of mercury. *Theoretical Chemistry Accounts* 129, 631–650. https://doi.org/10.1007/s00214-011-0911-2

Knecht, S., Repisky, M., Jensen, H.J.A., Saue, T. (2022) Exact two-component Hamiltonians for relativistic quantum chemistry: Two-electron picture-change corrections made simple. *The Journal of Chemical Physics* 157, 114106. https://doi.org/10.1063/5.0095112

Küchle, W., Dolg, M., Stoll, H., Preuss, H. (1994) Energy-adjusted pseudopotentials for the actinides. Parameter sets and test calculations for thorium and thorium monoxide. *The Journal of Chemical Physics* 100, 7535–7542. https://doi.org/10.1063/1.466847

Lee, C., Yang, W., Parr, R.G. (1988) Development of the Colle-Salvetti correlation-energy formula into a functional of the electron density. *Physical Review B* 37, 785–789. https://doi.org/10.1103/PhysRevB.37.785

Li, H., Tissot, F.L.H. (2023) UID: The uranium isotope database. *Chemical Geology* 618, 121221. https://doi.org/10.1016/j.chemgeo.2022.121221

Liu, W. (2010) Ideas of relativistic quantum chemistry. *Molecular Physics* 108, 1679–1706. https://doi.org/10.1080/00268971003781571

Moynier, F., Fujii, T., Telouk, P. (2009) Mass-independent isotopic fractionation of tin in chemical exchange reaction using a crown ether. *Analytica Chimica Acta* 632, 234–239. https://doi.org/10.1016/j.aca.2008.11.015

Nomura, M., Higuchi, N., Fujii, Y. (1996) Mass Dependence of Uranium Isotope Effects in the U(IV)−U(VI) Exchange Reaction. *Journal of the American Chemical Society* 118, 9127–9130. https://doi.org/10.1021/ja954075s

Noordmann, J., Weyer, S., Montoya-Pino, C., Dellwig, O., Neubert, N., Eckert, S., Paetzel, M., Böttcher, M.E. (2015) Uranium and molybdenum isotope systematics in modern euxinic basins: Case studies from the central Baltic Sea and the Kyllaren fjord (Norway). *Chemical Geology* 396, 182–195. https://doi.org/10.1016/j.chemgeo.2014.12.012

Richter, S., Eykens, R., Kühn, H., Aregbe, Y., Verbruggen, A., Weyer, S. (2010) New average values for the $n(^{238}U)/n(^{235}U)$ isotope ratios of natural uranium standards. *International Journal of Mass Spectrometry* 295, 94–97. https://doi.org/10.1016/j.ijms.2010.06.004

Sato, A., Bernier-Latmani, R., Hada, M., Abe, M. (2021) Ab initio and steady-state models for uranium isotope fractionation in

multi-step biotic and abiotic reduction. *Geochimica et Cosmochimica Acta* 307, 212–227. https://doi.org/10.1016/j.gca.2021.05.044

Saue, T. (2011) Relativistic Hamiltonians for Chemistry: A Primer. *ChemPhysChem* 12, 3077–3094. https://doi.org/10.1002/cphc.201100682

Saue, T., Bast, R., Gomes, A.S.P., Jensen, H.J.A., Visscher, L., *et al*. (2020) The DIRAC code for relativistic molecular calculations. *The Journal of Chemical Physics* 152, 204104. https://doi.org/10.1063/5.0004844

Scalmani, G., Frisch, M.J. (2010) Continuous surface charge polarizable continuum models of solvation. I. General formalism. *The Journal of Chemical Physics* 132, 114110. https://doi.org/10.1063/1.3359469

Scott, K.M., Lu, X., Cavanaugh, C.M., Liu, J.S. (2004) Optimal methods for estimating kinetic isotope effects from different forms of the Rayleigh distillation equation. *Geochimica et Cosmochimica Acta* 68, 433–442. https://doi.org/10.1016/S0016-7037(03)00459-9

Stephens, P.J., Devlin, F.J., Chabalowski, C.F., Frisch, M.J. (1994) Ab Initio Calculation of Vibrational Absorption and Circular Dichroism Spectra Using Density Functional Force Fields. *The Journal of Physical Chemistry* 98, 11623–11627. https://doi.org/10.1021/j100096a001

Stylo, M., Neubert, N., Wang, Y., Monga, N., Romaniello, S.J., Weyer, S., Bernier-Latmani, R. (2015) Uranium isotopes fingerprint biotic reduction. *Proceedings of the National Academy of Sciences* 112, 5619–5624. https://doi.org/10.1073/pnas.1421841112

Visscher, L., Dyall, K.G. (1997) Dirac–Fock atomic electronic structure calculations using different nuclear charge distributions. *Atomic Data and Nuclear Data Tables* 67, 207–224. https://doi.org/10.1006/adnd.1997.0751

Weyer, S., Anbar, A.D., Gerdes, A., Gordon, G.W., Algeo, T.J., Boyle, E.A. (2008) Natural fractionation of $^{238}U/^{235}U$. *Geochimica et Cosmochimica Acta* 72, 345–359. https://doi.org/10.1016/j.gca.2007.11.012

Young, E.D., Galy, A., Nagahara, H. (2002) Kinetic and equilibrium mass-dependent isotope fractionation laws in nature and their geochemical and cosmochemical significance. *Geochimica et Cosmochimica Acta* 66, 1095–1104. https://doi.org/10.1016/S0016-7037(01)00832-8

Zheng, W., Hintelmann, H. (2010) Nuclear Field Shift Effect in Isotope Fractionation of Mercury during Abiotic Reduction in the Absence of Light. *The Journal of Physical Chemistry A* 114, 4238–4245. https://doi.org/10.1021/jp910353y